

# Anomalous couplings in $Z\gamma$ events at NNLO+PS and improving $\nu\bar{\nu}\gamma$ backgrounds in dark-matter searches

Daniele Lombardi, Marius Wiesemann, and Giulia Zanderighi

Max-Planck-Institut für Physik, Föhringer Ring 6, 80805 München, Germany

[lombardi@mpp.mpg.de](mailto:lombardi@mpp.mpg.de)  
[marius.wiesemann@mpp.mpg.de](mailto:marius.wiesemann@mpp.mpg.de)  
[zanderi@mpp.mpg.de](mailto:zanderi@mpp.mpg.de)

## Abstract

The measurement of the triple gauge couplings (TGCs) is a central part of diboson studies at the LHC. In this letter we consider the  $Z\gamma$  process and include anomalous TGCs (aTGCs) in the event generation at next-to-next-to-leading order QCD accuracy (NNLO+PS) within the MINNLO<sub>PS</sub> framework. While our implementation is fully general and applies to both  $Z \rightarrow \ell^+\ell^-$  and  $Z \rightarrow \nu\bar{\nu}$  decays, we focus here on the  $\nu\bar{\nu}\gamma$  final state. After validation of our simulation of  $\nu\bar{\nu}\gamma$  events, for which NNLO+PS accuracy is achieved for the first time, the effects of aTGCs on various distributions are studied. Moreover, we show the relevance of NNLO+PS accuracy for the  $\nu\bar{\nu}\gamma$  background to photon plus missing energy signatures in dark-matter searches, and we compare MINNLO<sub>PS</sub> predictions for  $\nu\bar{\nu}\gamma$  production to recent 13 TeV data.

Precision phenomenology has evolved to one of the cornerstones of the rich physics programme at the Large Hadron Collider (LHC). Without a clear signal of new-physics phenomena, the accurate measurement of rates and distributions of Standard Model (SM) processes provides a potential pathway towards the discovery of physics beyond the SM (BSM) through small deviations from the SM predictions. Vector-boson pair production processes represent an important family of reactions in that respect, as they provide direct access to anomalous couplings between three gauge bosons (anomalous triple gauge coupling, or aTGC). Constraining or finding anomalous couplings profits directly from high-accuracy computations in perturbation theory. Indeed an enormous effort in the recent years has been spent on next-to-next-to-leading order (NNLO) QCD calculations, which are the standard today for colour-singlet production involving up to two bosons [1–33]. Within the last two years even the first  $2 \rightarrow 3$  LHC processes have been computed at NNLO QCD, namely  $\gamma\gamma\gamma$  [34, 35]  $\gamma\gamma$ +jet [36] and 3-jet [37] production. Indeed, in almost all cases NNLO corrections turn out to be crucial to accurately describe data from LHC measurements within the experimental uncertainties.

The production of a  $Z$  boson and a photon ( $Z\gamma$  production) is an important vector-boson pair production process in various respects. First of all, the measurement of non-zero  $ZZ\gamma$  or  $Z\gamma\gamma$  couplings, which are absent in the SM, would be direct evidence of BSM physics. Moreover,  $Z\gamma$  final states are relevant in direct searches for BSM particles. In particular, in the  $Z \rightarrow \nu\bar{\nu}$  decay channel  $Z\gamma$  production constitutes an irreducible background to dark-matter searches in the photon

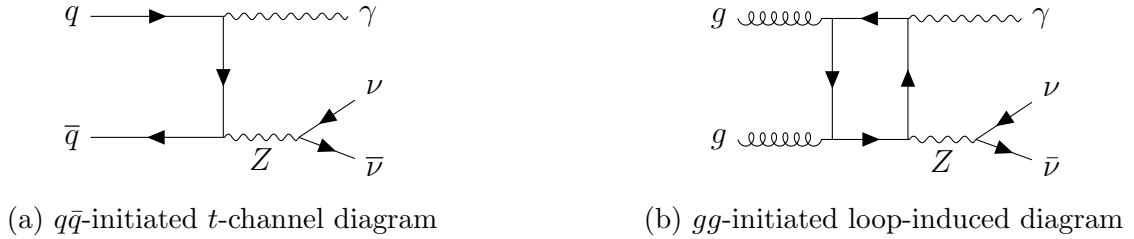


Figure 1: Sample Feynman diagrams for  $\nu\bar{\nu}\gamma$  production entering at (a) LO and (b) NNLO.

plus missing energy final state. The low accuracy of available  $\nu\bar{\nu}\gamma$  event simulations is actually one of the limiting factors in current dark-matter analyses [38], despite the fact that a substantial effort has been made to improve the perturbative accuracy of  $Z\gamma$  production. Next-to-leading order (NLO) QCD corrections have been known for a long time for on-shell  $Z$  bosons [39] and including their leptonic decays [40, 41]. Also the NNLO QCD cross section has been calculated at the fully differential level and including leptonic decays [16–18] as well as NLO electroweak (EW) corrections [42, 43]. More recently, the resummation of large logarithmic corrections for this process has been combined with NNLO QCD predictions [44–46].

In this letter we consider  $Z\gamma$  production in the  $Z \rightarrow \nu\bar{\nu}$  decay channel, and we present NNLO QCD predictions matched to parton showers (NNLO+PS) for the  $\nu\bar{\nu}\gamma$  final state. This calculation extends the list of LHC production processes available at NNLO+PS, which includes Higgs-boson [47–50], Drell-Yan [49–53], Higgsstrahlung [54–56],  $\gamma\gamma$  [57],  $\ell^+\ell^-\gamma$  [58],  $\ell^\pm\nu\gamma$  [59],  $\ell^+\nu\ell^-\nu\ell^-$  [60],  $\ell^+\ell^-\ell^+\ell^-$  [61, 62] and  $t\bar{t}$  production [63] so far. These simulations rely on overall four different NNLO+PS approaches that were developed in the last years [49–51, 63–65]. Our calculation employs the MINNLO<sub>PS</sub> approach of Refs. [49, 50] and it is based on the  $Z\gamma$  MINNLO<sub>PS</sub> generator for  $\ell^+\ell^-\gamma$  production presented in Ref. [58]. To the purpose of our study, we have extended the previous implementation to deal with the  $\nu\bar{\nu}\gamma$  final state and we have included in the event generation the effects of aTGCs, specifically the  $ZZ\gamma$  and  $Z\gamma\gamma$  vertices.<sup>1</sup>

We recall that MINNLO<sub>PS</sub> is a powerful approach with various positive features: NNLO corrections are calculated directly during event generation, without the need for an a-posteriori reweighting. Moreover, no merging scale or slicing cutoff is required to separate different multiplicities in the generated event samples, keeping power-suppressed terms into account. The leading-logarithmic accuracy of the shower is preserved when combined with transverse-momentum ordered parton showers. Although the MINNLO<sub>PS</sub> method has been initially developed on basis of the transverse momentum of colour singlet, the idea behind the approach is neither limited to a specific observable nor to colour-singlet production. Indeed, the method has recently been extended to heavy-quark pair production in Ref. [63].

We consider the process

$$pp \rightarrow \nu\bar{\nu}\gamma + X, \quad (1)$$

with  $\nu \in \{\nu_e, \nu_\mu, \nu_\tau\}$  and by accounting for all relevant topologies leading to this final state in our calculation, we include interferences, off-shell effects and spin correlations. At leading order (LO), the process is quark–anti-quark ( $q\bar{q}$ ) induced in the SM and proceeds only via a  $t$ -channel quark

<sup>1</sup>Although we study the  $\nu\bar{\nu}\gamma$  process here, the implementation of the aTGCs can readily be used to include those effects in the  $\ell^+\ell^-\gamma$  event generation at NNLO+PS as well.

exchange with both the isolated photon and the  $Z$  boson coupling to the quark line. This is different from the  $\ell^+\ell^-\gamma$  final state, where Drell-Yan-like  $s$ -channel topologies are allowed as well, since the charged leptons can emit an isolated photon, while the neutrinos can not. A representative LO Feynman diagram is shown in Figure 1(a). At NNLO in QCD perturbation theory the loop-induced gluon-fusion ( $gg$ ) contribution enters the cross section, see Figure 1(b). However, this contribution is very small – at the (sub-)percent level – and will be neglected throughout this letter, as it can be calculated completely independently from the  $q\bar{q}$  initiated process.

We calculate NNLO+PS predictions for the process in Eq. (1) by means of the `MINNLOPS` method. Our implementation is based on the  $Z\gamma$  `MINNLOPS` generator developed in Ref. [58], which has been extended to the  $\nu\bar{\nu}\gamma$  final state. As for the  $\ell^+\ell^-\gamma$  final state discussed in Ref. [58], tree-level and one-loop amplitudes can be evaluated either through an analytic implementation taken from MCFM [66] or through `OPENLOOPS` [67–69], while for the two-loop amplitude we rely on its implementation within the `MATRIX` framework [70, 71] that is based on the calculation of Ref. [72].<sup>2</sup> The `MINNLOPS` method has been formulated in Ref. [49], optimised for  $2 \rightarrow 1$  processes in Ref. [50] and later extended to generic colour-singlet processes in Ref. [58] and to heavy-quark pair production in Ref. [63]. We refer to those publications for details. The `MINNLOPS` master formula can be symbolically expressed through the `POWHEG` [73–76] formula for the production of a system of colour singlets (F) plus one light parton (FJ):

$$d\sigma_{\text{F}}^{\text{MiNNLO}_{\text{PS}}} = \bar{B}^{\text{MiNNLO}_{\text{PS}}} \times \left\{ \Delta_{\text{pwg}}(\Lambda_{\text{pwg}}) + \int d\Phi_{\text{rad}} \Delta_{\text{pwg}}(p_{T,\text{rad}}) \frac{R_{\text{FJ}}}{B_{\text{FJ}}} \right\}, \quad (2)$$

with a modified content of the  $\bar{B}$  function

$$\bar{B}^{\text{MiNNLO}_{\text{PS}}} \sim e^{-S} \left\{ d\sigma_{\text{FJ}}^{(1)} (1 + S^{(1)}) + d\sigma_{\text{FJ}}^{(2)} + (D - D^{(1)} - D^{(2)}) \times F^{\text{corr}} \right\}, \quad (3)$$

which ensures that that NNLO accuracy for F production is achieved when the additional jet becomes unresolved. In Eq. (2) we denote with  $\Delta_{\text{pwg}}$  the `POWHEG` Sudakov form factor, and with  $\Phi_{\text{rad}}$  and  $p_{T,\text{rad}}$  the phase space and the transverse momentum of the second radiation.  $B_{\text{FJ}}$  and  $R_{\text{FJ}}$  are the squared tree-level matrix elements for FJ and FJJ production, respectively.  $d\sigma_{\text{FJ}}^{(1,2)}$  in Eq. (3) are the first- and second-order contribution to the differential FJ cross section and  $e^{-S}$  denotes the Sudakov form factor for the transverse momentum ( $p_T$ ) of the colour singlet. The renormalization and factorization scales are evaluated as  $\mu_{\text{R}} \sim \mu_{\text{F}} \sim p_T$  in `MINNLOPS`. NNLO accuracy is achieved through the third term in Eq. (3), which adds the relevant (singular) contributions of order  $\alpha_s^3(p_T)$  [49]. Regular contributions at this order are of subleading nature. Those contributions are derived from the (fully differential) transverse-momentum resummation formula that can be written (approximately in direct space) as

$$d\sigma_{\text{F}}^{\text{res}} = \frac{d}{dp_T} \{ e^{-S} \mathcal{L} \} = e^{-S} \underbrace{\{ -S' \mathcal{L} + \mathcal{L}' \}}_{\equiv D}, \quad (4)$$

which defines the function  $D$  in Eq. (3). Here,  $\mathcal{L}$  is the luminosity factor up to NNLO including the convolution of the collinear coefficient functions with the parton distribution functions (PDFs) and the squared hard-virtual matrix elements for F production up to two-loop order. In fact, Eq. (3) follows directly from the matching of Eq. (4) to the fixed-order cross section  $d\sigma_{\text{FJ}}$  in a matching

<sup>2</sup>Note that we have corrected a minor sign mistake in the analytic continuation of a complex logarithm entering the two-loop quark form factor in `MATRIX`.



Figure 2: Anomalous couplings between three gauge bosons that are relevant for  $Z\gamma$  production.

scheme where the Sudakov form factor is factored out. Finally,  $F^{\text{corr}}$  in Eq. (3) represents the appropriate function to spread the NNLO corrections in the FJ phase space, which is necessary to include those corrections in the context of the FJ POWHEG calculation.

In summary, the MINNLO<sub>PS</sub> procedure involves essentially three steps: first, the FJ final state is described at NLO accuracy using POWHEG, inclusively over the radiation of a second light parton. Second, the limit in which the light partons become unresolved is corrected by supplementing the appropriate Sudakov form factor and higher-order terms, such that the simulation remains finite as well as NNLO accurate for inclusive F production. These first two steps are included in the  $\bar{B}$  function of Eq. (3). Third, the second radiation is generated exclusively through the content of the curly brackets in Eq. (2), with a default cutoff of  $\Lambda_{\text{pwg}} = 0.89 \text{ GeV}$ , preserving the NLO accuracy of FJ production, and subsequent radiation is included through the parton shower. We stress that MINNLO<sub>PS</sub> preserves the (leading logarithmic) accuracy of the parton shower, since the analytic Sudakov matches the leading logarithms generated by the parton shower itself and since all emissions are appropriately ordered (when matching to a  $p_T$ -ordered shower).

The ensuing calculation allows us to retain NNLO QCD accuracy in the event generation for  $\nu\bar{\nu}\gamma$  production interfaced to a parton shower, which is necessary for a complete and realistic event simulation. In particular, multiple photon emissions through a QED shower, as well as non-perturbative QCD effects using hadronization and underlying event models can be included. It is well known that these corrections can have a substantial impact on the lepton momenta, jet-binned cross sections and other more exclusive observables measured at the LHC.

In addition to the SM simulation, we have implemented the leading contributions from aTGCs in the  $Z\gamma$  MINNLO<sub>PS</sub> generator for both the  $\ell^+\ell^-\gamma$  and the  $\nu\bar{\nu}\gamma$  final states, but we will focus on the latter when presenting phenomenological results below. Since couplings between three charge-neutral weak bosons are forbidden by the SM gauge symmetry, their contributions can arise only from BSM theories. This is one of the reasons why they provide a powerful way of searching for new physics. Extensions of the standard model gauge structure through aTGC can be described by means of two equivalent approaches [77–80]: the vertex-function and the Lagrangian approach. Both descriptions can be embedded in a self-consistent effective-field-theory (EFT) framework, as presented in Refs. [81, 82]. Here, we follow the vertex-function approach, as this is usually employed by the experimental analyses, see for instance Ref. [83].

For  $Z\gamma$  production, two different neutral aTGCs enter the cross section, namely  $Z\gamma V$  with  $V = Z^*, \gamma^*$ , which are shown in Fig 2. The form of these effective interactions can be constraint by imposing Lorentz and electromagnetic gauge invariance, as well as Bose statistics. The latter for instance forbids vertices such as  $Z\gamma Z^*$  or  $Z\gamma\gamma^*$  with all gauge bosons being on-shell, since in

either case two identical particles are involved in the interaction. Moreover, we include only terms of dimension less than or equal to eight for practical reasons, as discussed in Ref. [78]. This choice, which avoids the proliferation of couplings that are in principle allowed by symmetry, is justified from an EFT perspective, where only a limited amount of higher-dimensional operators is expected to contribute to the physical process at a given energy scale. With these minimal requirements, the effective interaction can be parametrized as [79]:

$$\Gamma_{Z\gamma V}^{\alpha\beta\mu}(q_1, q_2, p) = \frac{i(p^2 - m_V^2)}{\Lambda^2} \left( h_1^V (q_2^\mu g^{\alpha\beta} - q_2^\alpha g^{\mu\beta}) + \right. \\ \left. + \frac{h_2^V}{\Lambda^2} p^\alpha (p \cdot q_2 g^{\mu\beta} - q_2^\mu p^\beta) - h_3^V \varepsilon^{\mu\alpha\beta\nu} q_{2\nu} - \frac{h_4^V}{\Lambda^2} \varepsilon^{\mu\beta\nu\sigma} p^\alpha p_\nu q_{2\sigma} \right), \quad (5)$$

where  $q_1$  and  $q_2$  are the momenta of the on-shell  $Z$  and  $\gamma$  gauge bosons, respectively, and  $p$  is the momentum of the off-shell boson  $V$ . One should bear in mind that in principle additional terms arise when all gauge bosons are considered to be off shell. However, since the  $Z\gamma$  analyses select isolated photons and measure predominantly contributions from  $Z$  bosons close to their mass shell, Eq. (5) provides the dominant effects also when including the leptonic decay of the final-state  $Z$  boson. The two anomalous vertices  $Z\gamma Z^*$  and  $Z\gamma\gamma^*$  are obtained by choosing the  $V = Z^*, \gamma^*$  and setting  $m_V^2$  accordingly. The effective couplings parametrizing the interaction are given by  $h_i^V$  with  $i \in \{1 \dots 4\}$  in Eq. (5) and  $\Lambda$  is a mass scale conventionally chosen to be the  $Z$  boson mass  $m_Z$ . Note that a different scale choice for  $\Lambda$  just amounts to a rescaling of all  $h_i^V$  couplings [77].

The  $h_1^V$  and  $h_2^V$  anomalous couplings are CP violating, and would only appear in a UV completion of the SM allowing for new particles with CP violating interactions with the SM ones. Being CP odd, these terms can not interfere with the SM sector and they can just contribute to the cross section at quadratic level. On the contrary, the CP-preserving couplings  $h_3^V$  and  $h_4^V$  enter the cross section also with linear terms through interference with the SM amplitudes. In principle one may think that this fact renders the CP-violating couplings more difficult to constrain [80]; however, the linear term involves an interference between the  $t$ -channel and  $s$ -channel diagrams (of the SM and BSM contribution, respectively), which is strongly suppressed. Note also that the experimental sensitivity is affected by the dimensionality of the coupling itself. In particular,  $h_{2/4}^V$  induce dimension eight terms, which grow with two extra powers of the energy scale with respect to the dimension six couplings  $h_{1/3}^V$ . Thus better limits can be obtained for  $h_{2/4}^V$  [80]. There are many explicit new-physics models that introduce such aTGCs, see Ref. [84] for instance. Indeed, any new fermionic particle can generate  $h_3^V$  at one-loop through a triangle diagram, while  $h_4^V$  arises only at a higher loop level or from non perturbative effects as in certain technicolour models.

Our implementation of aTGCs within the  $Z\gamma$  MINNLO<sub>PS</sub> generator follows closely the one in Ref. [18]. The relevant diagrams all involve  $q\bar{q}$ -initiated topologies where an (off-shell)  $Z$ -boson or photon is produced in the  $s$ -channel and splits into a  $Z$  boson and a photon through the anomalous vertices in Figure 2, with a subsequent decay of the  $Z$  boson (into charged leptons or neutrinos). We stress again that using Eq. (5) and considering the (off-shell) decay of the  $Z$  boson assumes that the experiments mostly measure  $Z$  bosons close to their mass shell, which is indeed a reasonable assumption. The relevant tree-level and one-loop amplitudes have been taken from MCFM [66], while we extended the calculation of the  $q\bar{q} \rightarrow \ell^+ \ell^- \gamma$  and  $q\bar{q} \rightarrow \nu \bar{\nu} \gamma$  two-loop helicity amplitudes of Ref. [72] with the relevant anomalous contributions directly within MATRIX [67–69], using the  $q\bar{q}V^*$  form factor [85–87] for the loop corrections to the tree-level amplitudes with aTGCs.

	fiducial-setup-1	fiducial-setup-2	DM-setup
Photon cuts	$p_{T,\gamma} > 100 \text{ GeV}$ $ \eta_\gamma  < 2.37$	$p_{T,\gamma} > 150 \text{ GeV}$ $ \eta_\gamma  < 2.37$	$p_{T,\gamma} > 150 \text{ GeV}$ $ \eta_\gamma  < 1.37$ or $1.52 <  \eta_\gamma  < 2.37$ $\Delta\phi_{\gamma,\vec{p}_{T,\text{miss}}} > 0.4$
Neutrino cuts	$p_{T,\text{miss}} > 90 \text{ GeV}$	$p_{T,\text{miss}} > 150 \text{ GeV}$	$p_{T,\text{miss}} > 200 \text{ GeV}$
Jet cuts	—	Inclusive: $N_{\text{jet}} \geq 0$ Exclusive: $N_{\text{jet}} = 0$	$N_{\text{jet}} \leq 1$
Jet definition	anti- $k_T$ with $R = 0.4$ $p_{T,j} > 30 \text{ GeV}$ $ \eta_j  < 4.4$ $\Delta R_{\gamma j} > 0.3$	anti- $k_T$ with $R = 0.4$ $p_{T,j} > 50 \text{ GeV}$ $ \eta_j  < 4.5$ $\Delta R_{\gamma j} > 0.3$	anti- $k_T$ with $R = 0.4$ $p_{T,j} > 30 \text{ GeV}$ $ \eta_j  < 4.5$ $\Delta\phi_{j,\vec{p}_{T,\text{miss}}} > 0.4$
Photon Isolation	Frixione isolation $n = 1$ $\epsilon_\gamma = 0.5$ $\delta_0 = 0.4$	Frixione isolation $n = 1$ $\epsilon_\gamma = 0.1$ $\delta_0 = 0.1$	Frixione isolation $n = 1$ $E_T^{\text{ref}} = 2.45 \text{ GeV} + 0.022 p_{T,\gamma}$ $\delta_0 = 0.4$

Table 1: Definition of fiducial cuts of two ATLAS measurements, **fiducial-setup-1** [89] and **fiducial-setup-2** [83], and of the **DM-setup** that is inspired by the dark-matter search of Ref. [38].

We now turn to presenting phenomenological results for  $pp \rightarrow \nu\bar{\nu}\gamma$  production at the LHC with  $\sqrt{s} = 13 \text{ TeV}$  centre-of-mass energy for  $\nu \in \{\nu_e, \nu_\mu, \nu_\tau\}$ . All results have been obtained with  $N_f = 5$  massless quark flavours and the corresponding NNLO set of the NNPDF3.0 [88] parton distribution functions (PDFs) with a strong coupling  $\alpha_s(m_Z) = 0.118$ . The electroweak parameters are evaluated in the  $G_\mu$  scheme with the electroweak coupling  $\alpha_{G_\mu} = \sqrt{2}G_\mu m_W^2 \sin^2 \theta_W / \pi$  and the mixing angle  $\cos^2 \theta_W = m_W^2 / m_Z^2$ . The input parameters are set to  $G_\mu = 1.16637 \times 10^{-5} \text{ GeV}^{-2}$ ,  $m_Z = 91.1876 \text{ GeV}$ ,  $m_W = 80.385 \text{ GeV}$ ,  $\Gamma_Z = 2.4952 \text{ GeV}$ , and  $\Gamma_W = 2.085 \text{ GeV}$ . The scale setting for MINNLO<sub>PS</sub> (MINLO') is fixed by the method itself and it is the same as in Ref. [58]. In the fixed-order results we set the central renormalization and factorization scales to the transverse mass of the  $Z\gamma$  system. In all cases we use 7-point scale variations to estimate the uncertainties related to missing higher-order contributions.

We consider three sets of fiducial cuts in this letter, which are summarized in Table 1. The first one (**fiducial-setup-1**) corresponds to an earlier ATLAS analysis [89] and is used for validation purposes. To study the effects of aTGCs we use **fiducial-setup-2**, which is also employed to compare MINNLO<sub>PS</sub> predictions to a recent  $\nu\bar{\nu}\gamma$  measurement by ATLAS [83]. The last setup (**DM-setup**) has instead been chosen to study the importance of NNLO+PS predictions for reducing the uncertainties of the  $\nu\bar{\nu}\gamma$  background in dark-matter searches in the photon plus missing energy channel and it is inspired by a recent dark-matter search [38]. All three setups include standard cuts on the identified photon and the missing transverse energy, a jet definition and Frixione smooth-cone isolation [90] for the photon (see Ref. [58] for our notation). In **fiducial-setup-2** one category inclusive over QCD radiation and one with a jet veto is considered. The **DM-setup**,

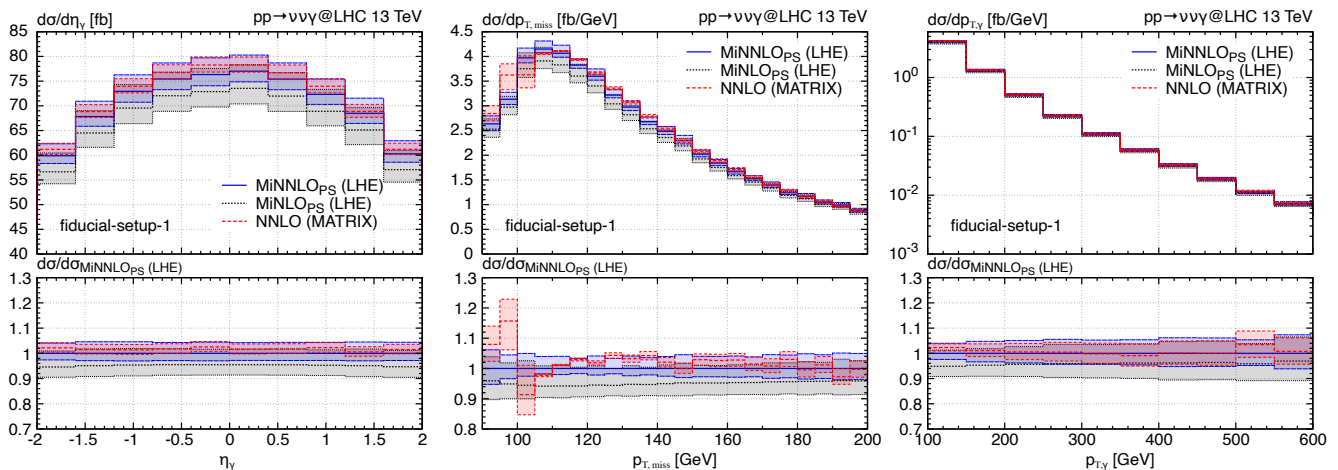


Figure 3: Selected plots at LHE level for validation of  $\text{MiNNLO}_{\text{PS}}$  against NNLO.

on the other hand, considers a quite special choice for the smooth-cone parameters as it combines a fixed (lower) threshold with a fraction of the photon transverse momentum, c.f. Eqs. (2.8) and (2.9) of Ref. [58]. Note also that in the  $\text{DM-setup}$  various categories in  $p_{\text{T,miss}}$  are considered, as discussed below, where the  $p_{\text{T,miss}}$  cut given in Table 1 is just the loosest one.

In Figure 3 we start by comparing  $\text{MiNNLO}_{\text{PS}}$  (blue, solid line),  $\text{MiNLO}'$  (black, dotted line), and fixed-order NNLO predictions (red, dashed line). This comparison is done at the Les-Houches-Event (LHE) level and it serves the purpose of numerically validating the NNLO accuracy of the  $\text{MiNNLO}_{\text{PS}}$  predictions as well as indicating the importance of NNLO corrections and matching to the parton shower. The left plot shows the rapidity distribution of the photon. The agreement between  $\text{MiNNLO}_{\text{PS}}$  and NNLO predictions is excellent, with fully overlapping uncertainty bands. We remind the reader that small differences (within uncertainties) between  $\text{MiNNLO}_{\text{PS}}$  and fixed-order results are expected due to the different scale settings and treatment of terms beyond accuracy, see Ref. [58] for instance. Moreover, when performing scale variations for  $\text{MiNLO}'$  and  $\text{MiNNLO}_{\text{PS}}$ , an additional scale dependence is kept in the Sudakov form factor [49] for a more conservative uncertainty estimate, which is absent in fixed-order calculations. This is reflected in the slightly larger  $\text{MiNNLO}_{\text{PS}}$  uncertainty band. Compared to  $\text{MiNLO}'$ , however, we observe a clear reduction of scale uncertainties from about 6% to 3% for  $\text{MiNNLO}_{\text{PS}}$  and roughly an effect of +3% in normalization from the inclusion of NNLO corrections through  $\text{MiNNLO}_{\text{PS}}$ . Also, at high values of the missing energy ( $p_{\text{T,miss}}$ ) and of the transverse momentum of the photon ( $p_{\text{T},\gamma}$ ) Figure 3 shows that  $\text{MiNNLO}_{\text{PS}}$  and fixed-order NNLO predictions are in excellent agreement. At small values of the missing transverse energy, on the other hand, we observe that the NNLO curve develops an interesting feature. This is a consequence of the fiducial cut of  $p_{\text{T},\gamma} > 100$  GeV, which induces a perturbative instability [91] in  $p_{\text{T,miss}}$  at the threshold, as the region  $p_{\text{T,miss}} \leq 100$  GeV becomes sensitive to soft-gluon effects and is effectively filled only starting from NLO. This behaviour of fixed-order predictions is unphysical and cured in  $\text{MiNNLO}_{\text{PS}}$  (already at LHE level).

We continue by studying the effects of aTGCs on differential distributions. The search for aTGCs in  $Z\gamma$  production has received great attention in the past, both at the Tevatron [92, 93], and at the LHC at 7 TeV and 8 TeV [89, 94–100]. We stress that, the  $Z \rightarrow \bar{\nu}\nu$  decay channel has a higher sensitivity to aTGCs due to its higher branching ratio than the  $Z \rightarrow \ell^+\ell^-$  decay channel. Indeed,

the most recent 13 TeV ATLAS analysis [83] uses the  $\nu\bar{\nu}\gamma$  final state to set the most stringent limits on the aTGCs under consideration thus far, which are of the order of  $\pm 10^{-4}$  for  $h_3^V$  and  $\pm 10^{-7}$  for  $h_4^V$  (see Table 8 of [83] for the exact bounds). This ATLAS analysis did not make use of any form-factor suppression, which is sometimes applied to prevent unitarity violation at high energy, caused by the introduction of aTGCs at the amplitude level [101]. Indeed, in an EFT perspective the terms entering the vertex function in Eq. (5) would arise from a set of gauge-invariant operators at dimension-eight (or higher) [82], whose validity range is limited by the given new-physics scale. Here, we also refrain from using any form-factor suppression.

Different combinations of the aTGCs have been obtained through reweighting at event-generation level (i.e stage 4 in POWHEG), while ensuring sufficient statistics in the relevant phase space regions by accounting for the resonance structure of both the  $t$ -channel SM and  $s$ -channel BSM topologies and by applying a suitable suppression factor to increase the sampling in the high energy tails.<sup>3</sup> Even though all eight anomalous couplings ( $h_i^V$  with  $i \in \{1..4\}$  and  $V \in \{Z, \gamma\}$ ) are consistently implemented in our code, we limit our study to the CP conserving ones, which do not interfere with the CP violating ones. Moreover, since also the  $V = Z$  and  $V = \gamma$  couplings have been shown to only mildly interfere with each other [77] and to have qualitatively a very similar impact, we focus on the pair  $(h_3^Z, h_4^Z)$  here. The most relevant phase-space regions to constrain aTGCs in  $\nu\bar{\nu}\gamma$  production are the high-energy tails of the  $p_{T,\text{miss}}$  and  $p_{T,\gamma}$  spectra. In Figure 4 we show MINNLO<sub>PS</sub> predictions of each of these two observables in `fiducial-setup-2` with a jet veto ( $N_{\text{jet}} = 0$ ), which is experimentally applied to reduce the SM background in the tails of the distributions. MINNLO<sub>PS</sub> results include parton shower and hadronization effects as provided by PYTHIA8 [102], with the A14 tune [103]. We present individual variations of  $h_3^Z$  (two upper plots), individual variations of  $h_4^Z$  (two central plots), and combinations of  $(h_3^Z, h_4^Z)$  (two bottom plots), all within the currently allowed limits [83]. In all plots, the SM results ( $h_3^Z = 0, h_4^Z = 0$ ) are shown with a blue, solid line. As one sees from the individual variations of  $h_3^Z$  and  $h_4^Z$ , both negative and positive values of the aTGCs lead to a similar positive effect on the spectra, which is a consequence of the very small interference of the  $s$ -channel BSM amplitudes with the  $t$ -channel SM amplitude, so that the quadratic term in the anomalous couplings dominates. This is also the reason why the experimental limits on the aTGCs in  $Z\gamma$  production are almost symmetric. For values of  $h_3^Z$  at the edges of experimentally allowed ranges, we start observing deviations of 5-10% from the SM for transverse momentum values of 400-500 GeV, with a steep increase afterwards, reaching already 100% around 700-800 GeV. For  $h_4^Z$ , whose constraints are at least three order of magnitude smaller, 5-10% effects in the tails of transverse momentum distributions manifest themselves starting from 600-700 GeV, with rapidly increasing effects at larger  $p_T$  as well. Looking at the simultaneous variations of  $(h_3^Z, h_4^Z)$ , it is clear that different sign combinations constructively interfere, with a mild difference between the two possible sign combinations. On the other hand, same sign combinations of  $(h_3^Z, h_4^Z)$  interfere destructively.

Now we turn to discussing the importance of NNLO+PS predictions for  $\nu\bar{\nu}\gamma$  productions in the context of dark-matter searches in the photon plus missing energy ( $\gamma + E_{T,\text{miss}}$ ) channel, which is one of (if not the) most important signature to detect dark matter at the LHC, see Refs. [38, 104, 105]. Other  $X + E_{T,\text{miss}}$  signatures (where X is a visible particle) have been extensively studied at the LHC in the past years: for a jet ([106, 107]), for a heavy quark ([108, 109]), for a vector

---

<sup>3</sup>To this end, we have added the aTGC coefficients as inputs to the POWHEG reweighting information, introduced the flag `anommode 1` that enables the  $s$ -channel resonance histories associated with the aTGCs to be included through the `build_resonance_histories` routines of POWHEG-BOX-RES, and implemented a suitable suppression factor in the code that can be activated via `suppmode1 2`.



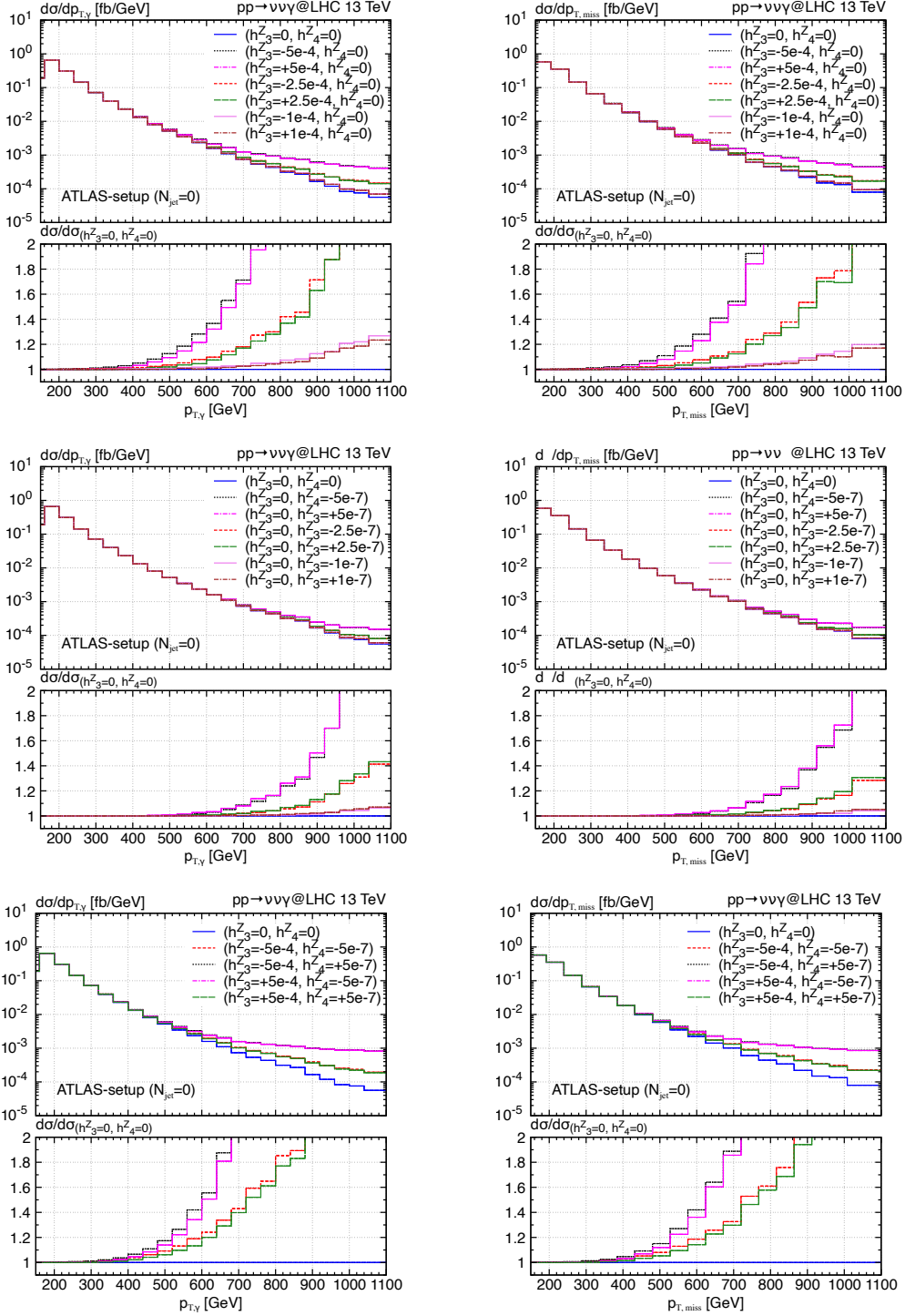


Figure 4: MiNNLO<sub>PS</sub> predictions for the photon transverse momentum (left column) and the missing transverse momentum (right column) for different values of  $h_3^Z$  and  $h_4^Z$ . The SM results are reported with a blue, solid line. Individual variations  $h_3^Z$  (two upper plots), individual variation of  $h_4^Z$  (two central plots) and their combined variation (two bottom plots) are considered for different values within the experimentally allowed ranges defined in Table 8 of [83]. All MiNNLO<sub>PS</sub> results include parton shower and hadronization effects, as provided by PYTHIA8.

category	SRI1	SRI2	SRI3	SRI4
$p_{T,\text{miss}}$ [GeV]	> 200	> 250	> 300	> 375
MINLO' [fb]	27.35(18) $^{+6.0\%}_{-3.5\%}$	12.95(11) $^{+6.5\%}_{-4.2\%}$	6.65(8) $^{+6.8\%}_{-4.7\%}$	2.77(6) $^{+8.0\%}_{-5.8\%}$
MINNLO <sub>PS</sub> [fb]	29.09(18) $^{+2.9\%}_{-1.9\%}$	13.77(12) $^{+3.2\%}_{-2.2\%}$	7.07(8) $^{+3.2\%}_{-2.4\%}$	2.95(6) $^{+4.2\%}_{-3.2\%}$

Table 2: Fiducial cross section in various inclusive  $p_{T,\text{miss}}$  categories in the DM-setup.

category	SRE1	SRE2	SRE3
$p_{T,\text{miss}}$ [GeV]	200–250	250–300	300–375
MINLO' [fb]	14.4(1.4) $^{+5.4\%}_{-3.2\%}$	6.30(8) $^{+6.2\%}_{-3.7\%}$	3.88(5) $^{+5.8\%}_{-3.9\%}$
MINNLO <sub>PS</sub> [fb]	15.32(15) $^{+2.7\%}_{-1.6\%}$	6.69(7) $^{+3.2\%}_{-2.0\%}$	4.12(5) $^{+2.5\%}_{-1.8\%}$

Table 3: Fiducial cross section in various exclusive  $p_{T,\text{miss}}$  categories in the DM-setup.

boson ([107, 110, 111]) and for a Higgs boson ([112, 113]). In Ref. [38], which is the most recent dark-matter study in the  $\gamma + E_{T,\text{miss}}$  channel, the results are interpreted both in terms of simplified dark matter models [114–116] and of effective field theories of axion-like particles (ALPs) [117]. As one can see from Table 4 and 5 of Ref. [38] for instance, the dominant SM background is the  $\nu\bar{\nu}\gamma$  process, which also dominates the uncertainties of the expected SM events. Depending on the category in  $p_{T,\text{miss}}$  considered in Ref. [38], which were used to improve the sensitivity of the analysis, the uncertainties on the expected  $\nu\bar{\nu}\gamma$  events range from 4% to almost 15%. Ref. [38] based its  $\nu\bar{\nu}\gamma$  predictions on a merged calculation of 0-jet and 1-jet events at NLO+PS within the Sherpa 2.2 MC event generator ([118, 119]).

Here, we consider MINLO' predictions, which have the same formal accuracy as the merged Sherpa 2.2 results quoted in Ref. [38], and study the reduction of scale uncertainties when including MINNLO<sub>PS</sub> corrections in each  $p_{T,\text{miss}}$  category. Among the categories in  $p_{T,\text{miss}}$  considered in Ref. [38], four are of inclusive type (SRI1-SRI4) and three exclusive (SRE1-SRE3). The different  $p_{T,\text{miss}}$  ranges defining each of the seven categories are summarized in Table 2 and 3. These tables also report MINLO' and MINNLO<sub>PS</sub> predictions for the cross sections in those categories with the respective scale uncertainties. Also in this case, results have been showered using PYTHIA8, with the inclusion of hadronization effects. One should bear in mind that the experimental analysis is performed at the level of events measured in the detector, so that an immediate comparison to Table 4 and 5 of Ref. [38] is not possible. However, both the relative MINNLO<sub>PS</sub> correction and the reduction of scale uncertainties from MINLO' to MINNLO<sub>PS</sub> give a good indication of the expected improvements. Moreover, by and large, relative uncertainties at detector-event level and at the fiducial level can be assumed to be similar, so that even a direct comparison between our fiducial MINNLO<sub>PS</sub> results and Ref. [38] is not meaningless. We find roughly a 6% correction in the central value for all categories by including NNLO corrections through MINNLO<sub>PS</sub>. Moreover, even though uncertainties are larger in categories with more stringent cuts, we still observe an overall reduction in the uncertainty bands by roughly a factor of two. Comparing our uncertainties to the ones of the  $\nu\bar{\nu}\gamma$  backgrounds reported in Table 4 and 5 of Ref. [38], we find smaller uncertainties of

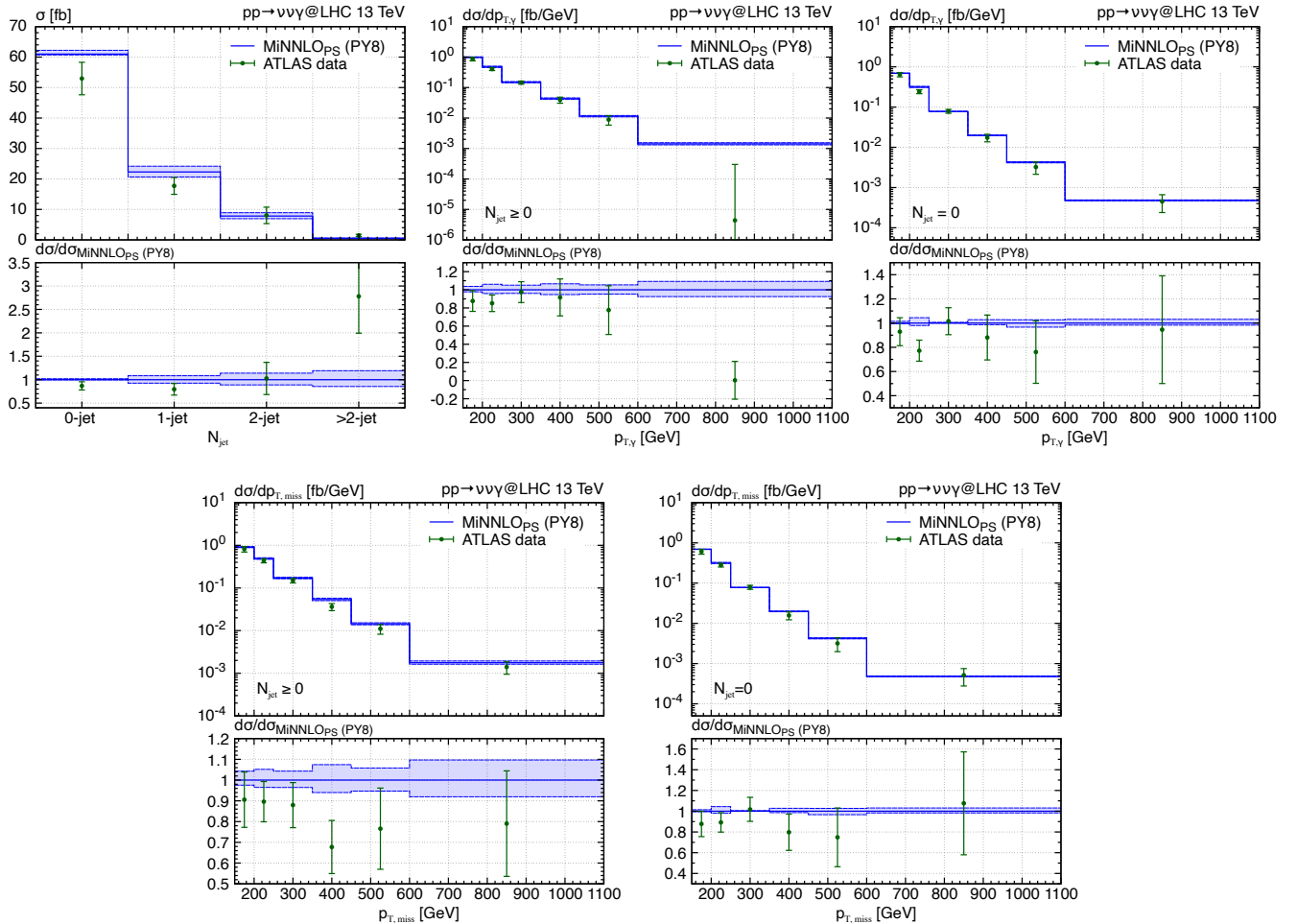


Figure 5: Distribution in the number of jets ( $N_{\text{jet}}$ ), in the transverse-momentum of the photon ( $p_{T,\gamma}$ ) and in the missing transverse momentum ( $p_{T,\text{miss}}$ ) compared to 13 TeV ATLAS data [83]. The latter two are shown both inclusively ( $N_{\text{jet}} \geq 0$ ) and with a jet veto ( $N_{\text{jet}} = 0$ ).

MINNLO<sub>PS</sub> already in the SRI1 category (+2.9% and −1.9% compared to ±4.4%), while with increasing  $p_{T,\text{miss}}$  cut the quoted uncertainties on the  $\nu\bar{\nu}\gamma$  events in Ref. [38] increase significantly, up to ±13% in SRI4, while our MINNLO<sub>PS</sub> uncertainties amount to less than 5%, bearing in mind that the translation of the uncertainties of the predictions at detector-event level to those at fiducial level is not immediate, as explained above. Similarly, in the exclusive  $p_{T,\text{miss}}$  categories in Table 3 the MINNLO<sub>PS</sub> uncertainties stay within about 3%, while the quoted uncertainties in Ref. [38] of the  $\nu\bar{\nu}\gamma$  predictions range from 6% to 9%. In conclusion, MINNLO<sub>PS</sub> predictions for  $\nu\bar{\nu}\gamma$  production will allow the experiments to substantially improve the dominant background uncertainty in dark-matter searches in the photon plus missing energy channel.

Finally, we compare our  $\nu\bar{\nu}\gamma$  MINNLO<sub>PS</sub> predictions, including the effects from hadronization, against ATLAS data [83] in Figure 5. The first plot shows the distribution in the number of jets. The agreement between the MINNLO<sub>PS</sub> results and the data points for the different jet cross sections is reasonable, being within at most two standard deviations. Note that, starting from NNLO accuracy for the 0-jet cross section, the accuracy of the MINNLO<sub>PS</sub> calculation decreases by one order for each jet multiplicity, with the > 2-jet multiplicity described only by the shower.

This is the reason why the prediction undershoots the data in this bin. The other plots in Figure 5 show the  $p_{T,\gamma}$  and  $p_{T,\text{miss}}$  spectra with and without a jet veto ( $N_{\text{jet}} = 0$ ). Also here the agreement between MINNLO<sub>PS</sub> predictions and data is very good, with deviations of typically one or at most two standard deviations. There is however one exception: the measured result in last bin in the inclusive ( $N_{\text{jet}} \geq 0$ )  $p_{T,\gamma}$  spectrum is many standard deviations away from the prediction. The data point seems to be way too low, when following the trend of the distribution. Indeed, it has a very large error and is actually compatible with zero. Moreover, looking at the  $N_{\text{jet}} = 0$  result, this bin has actually a higher measured cross section than in the inclusive case, which appears inconsistent considering the fact that the  $N_{\text{jet}} = 0$  cross section should be part of the  $N_{\text{jet}} \geq 0$  one. A possible explanation could be that, because of the additional jet activity, some events are discarded, for instance due to the photon isolation requirements. Indeed, looking at the  $p_{T,\text{miss}}$  spectrum no such behaviour is observed.

To summarize, we have presented the simulation of NNLO-accurate events for the  $Z\gamma$  process including the effects of anomalous triple gauge couplings. The calculation has been performed in the MINNLO<sub>PS</sub> framework and we have focused on the  $\nu\bar{\nu}\gamma$  final state, although the implementation applies also to the  $\ell^+\ell^-\gamma$  process. We followed the vertex-function approach for a consistent inclusion of the anomalous couplings, but one should bear in mind that there is a direct translation to an EFT framework [81, 82]. We validated our MINNLO<sub>PS</sub>  $\nu\bar{\nu}\gamma$  results numerically against fixed-order NNLO predictions, and we have demonstrated the importance of both NNLO accuracy and the matching to the parton shower in certain phase-space regimes. The effect of the CP-conserving aTGCs has been studied for the most relevant observables to extract anomalous couplings in  $\nu\bar{\nu}\gamma$  analyses. We found that quadratic terms yield the dominant contribution to the cross section and that the interference with the SM has a relatively small impact. This typically leads to very symmetric bounds on the respective coefficients extracted by the experiments. We have further shown that the simulation of NNLO-accurate  $\nu\bar{\nu}\gamma$  events in the SM is crucial to reduce the uncertainty on the dominant background in dark-matter searches in the photon plus missing energy channel. Our calculation provides an improvement over the previous scale uncertainties of merged  $\nu\bar{\nu}\gamma+0,1$ -jet predictions by a factor of two or more. Finally, the good agreement of MINNLO<sub>PS</sub> predictions with measured distributions underlines the importance of NNLO+PS predictions for  $\nu\bar{\nu}\gamma$  production. We believe that both the inclusion of aTGCs in our  $Z\gamma$  MINNLO<sub>PS</sub> generator and the implementation of the  $\nu\bar{\nu}\gamma$  final state will be very useful for future  $Z\gamma$  measurements as well as BSM searches using the photon plus missing energy signature for aTGCs and dark matter studies at the LHC.

**Acknowledgements.** We would like to thank William Bobadilla, Pier Francesco Monni, Paolo Nason, Emanuele Re, and Vasily Sotnikov for fruitful discussions. We have used the Max Planck Computing and Data Facility (MPCDF) in Garching to carry out all simulations presented here.

## References

- [1] G. Ferrera, M. Grazzini, and F. Tramontano, *Phys. Rev. Lett.* **107**, 152003 (2011), [arXiv:1107.1164 \[hep-ph\]](#) .
- [2] G. Ferrera, M. Grazzini, and F. Tramontano, *Phys. Lett.* **B740**, 51 (2015), [arXiv:1407.4747 \[hep-ph\]](#) .
- [3] G. Ferrera, G. Somogyi, and F. Tramontano, *Phys. Lett.* **B780**, 346 (2018), [arXiv:1705.10304 \[hep-ph\]](#) .

- [4] J. M. Campbell, R. K. Ellis, and C. Williams, *JHEP* **06**, 179 (2016), [arXiv:1601.00658 \[hep-ph\]](#) .
- [5] R. V. Harlander and W. B. Kilgore, *Phys. Rev.* **D68**, 013001 (2003), [arXiv:hep-ph/0304035 \[hep-ph\]](#) .
- [6] R. V. Harlander, K. J. Ozeren, and M. Wiesemann, *Phys. Lett.* **B693**, 269 (2010), [arXiv:1007.5411 \[hep-ph\]](#) .
- [7] R. Harlander and M. Wiesemann, *JHEP* **04**, 066 (2012), [arXiv:1111.2182 \[hep-ph\]](#) .
- [8] S. Bühler, F. Herzog, A. Lazopoulos, and R. Müller, *JHEP* **07**, 115 (2012), [arXiv:1204.4415 \[hep-ph\]](#) .
- [9] S. Marzani, R. D. Ball, V. Del Duca, S. Forte, and A. Vicini, *Nucl. Phys.* **B800**, 127 (2008), [arXiv:0801.2544 \[hep-ph\]](#) .
- [10] R. V. Harlander and K. J. Ozeren, *JHEP* **11**, 088 (2009), [arXiv:0909.3420 \[hep-ph\]](#) .
- [11] R. V. Harlander, H. Mantler, S. Marzani, and K. J. Ozeren, *Eur. Phys. J.* **C66**, 359 (2010), [arXiv:0912.2104 \[hep-ph\]](#) .
- [12] A. Pak, M. Rogal, and M. Steinhauser, *JHEP* **02**, 025 (2010), [arXiv:0911.4662 \[hep-ph\]](#) .
- [13] T. Neumann and M. Wiesemann, *JHEP* **11**, 150 (2014), [arXiv:1408.6836 \[hep-ph\]](#) .
- [14] S. Catani, L. Cieri, D. de Florian, G. Ferrera, and M. Grazzini, *Phys. Rev. Lett.* **108**, 072001 (2012), [arXiv:1110.2375 \[hep-ph\]](#) .
- [15] J. M. Campbell, R. K. Ellis, Y. Li, and C. Williams, *JHEP* **07**, 148 (2016), [arXiv:1603.02663 \[hep-ph\]](#) .
- [16] M. Grazzini, S. Kallweit, D. Rathlev, and A. Torre, *Phys. Lett.* **B731**, 204 (2014), [arXiv:1309.7000 \[hep-ph\]](#) .
- [17] M. Grazzini, S. Kallweit, and D. Rathlev, *JHEP* **07**, 085 (2015), [arXiv:1504.01330 \[hep-ph\]](#) .
- [18] J. M. Campbell, T. Neumann, and C. Williams, *JHEP* **11**, 150 (2017), [arXiv:1708.02925 \[hep-ph\]](#) .
- [19] T. Gehrmann, N. Glover, A. Huss, and J. Whitehead, *JHEP* **01**, 108 (2021), [arXiv:2009.11310 \[hep-ph\]](#) .
- [20] F. Cascioli, T. Gehrmann, M. Grazzini, S. Kallweit, P. Maierhöfer, A. von Manteuffel, S. Pozzorini, D. Rathlev, L. Tancredi, and E. Weihs, *Phys. Lett.* **B735**, 311 (2014), [arXiv:1405.2219 \[hep-ph\]](#) .
- [21] M. Grazzini, S. Kallweit, and D. Rathlev, *Phys. Lett.* **B750**, 407 (2015), [arXiv:1507.06257 \[hep-ph\]](#) .
- [22] G. Heinrich, S. Jahn, S. P. Jones, M. Kerner, and J. Pires, *JHEP* **03**, 142 (2018), [arXiv:1710.06294 \[hep-ph\]](#) .
- [23] S. Kallweit and M. Wiesemann, *Phys. Lett.* **B786**, 382 (2018), [arXiv:1806.05941 \[hep-ph\]](#) .
- [24] T. Gehrmann, M. Grazzini, S. Kallweit, P. Maierhöfer, A. von Manteuffel, S. Pozzorini, D. Rathlev, and L. Tancredi, *Phys. Rev. Lett.* **113**, 212001 (2014), [arXiv:1408.5243 \[hep-ph\]](#) .
- [25] M. Grazzini, S. Kallweit, S. Pozzorini, D. Rathlev, and M. Wiesemann, *JHEP* **08**, 140 (2016), [arXiv:1605.02716 \[hep-ph\]](#) .
- [26] M. Grazzini, S. Kallweit, D. Rathlev, and M. Wiesemann, *Phys. Lett.* **B761**, 179 (2016), [arXiv:1604.08576 \[hep-ph\]](#) .

- [27] M. Grazzini, S. Kallweit, D. Rathlev, and M. Wiesemann, *JHEP* **05**, 139 (2017), [arXiv:1703.09065 \[hep-ph\]](#) .
- [28] D. de Florian and J. Mazzitelli, *Phys. Rev. Lett.* **111**, 201801 (2013), [arXiv:1309.6594 \[hep-ph\]](#) .
- [29] D. de Florian, M. Grazzini, C. Hanga, S. Kallweit, J. M. Lindert, P. Maierhöfer, J. Mazzitelli, and D. Rathlev, *JHEP* **09**, 151 (2016), [arXiv:1606.09519 \[hep-ph\]](#) .
- [30] M. Grazzini, G. Heinrich, S. Jones, S. Kallweit, M. Kerner, J. M. Lindert, and J. Mazzitelli, *JHEP* **05**, 059 (2018), [arXiv:1803.02463 \[hep-ph\]](#) .
- [31] J. Baglio, A. Djouadi, R. Gröber, M. Mühlleitner, J. Quevillon, and M. Spira, *JHEP* **04**, 151 (2013), [arXiv:1212.5581 \[hep-ph\]](#) .
- [32] H. T. Li and J. Wang, *Phys. Lett. B* **765**, 265 (2017), [arXiv:1607.06382 \[hep-ph\]](#) .
- [33] D. de Florian, I. Fabre, and J. Mazzitelli, *JHEP* **03**, 155 (2020), [arXiv:1912.02760 \[hep-ph\]](#) .
- [34] H. A. Chawdhry, M. L. Czakon, A. Mitov, and R. Poncelet, *JHEP* **02**, 057 (2020), [arXiv:1911.00479 \[hep-ph\]](#) .
- [35] S. Kallweit, V. Sotnikov, and M. Wiesemann, *Phys. Lett. B* **812**, 136013 (2021), [arXiv:2010.04681 \[hep-ph\]](#) .
- [36] M. Czakon, A. Mitov, and R. Poncelet, (2021), [arXiv:2106.05331 \[hep-ph\]](#) .
- [37] H. A. Chawdhry, M. Czakon, A. Mitov, and R. Poncelet, (2021), [arXiv:2105.06940 \[hep-ph\]](#) .
- [38] G. Aad *et al.* (ATLAS), *JHEP* **02**, 226 (2021), [arXiv:2011.05259 \[hep-ex\]](#) .
- [39] J. Ohnemus, *Phys. Rev. D* **47**, 940 (1993).
- [40] U. Baur, T. Han, and J. Ohnemus, *Phys. Rev. D* **57**, 2823 (1998), [arXiv:hep-ph/9710416](#) .
- [41] J. M. Campbell, R. K. Ellis, and C. Williams, *JHEP* **07**, 018 (2011), [arXiv:1105.0020 \[hep-ph\]](#) .
- [42] W. Hollik and C. Meier, *Phys. Lett. B* **590**, 69 (2004), [arXiv:hep-ph/0402281](#) .
- [43] E. Accomando, A. Denner, and C. Meier, *Eur. Phys. J. C* **47**, 125 (2006), [arXiv:hep-ph/0509234](#) .
- [44] S. Kallweit, E. Re, L. Rottoli, and M. Wiesemann, *JHEP* **12**, 147 (2020), [arXiv:2004.07720 \[hep-ph\]](#) .
- [45] M. Wiesemann, L. Rottoli, and P. Torrielli, *Phys. Lett. B* **809**, 135718 (2020), [arXiv:2006.09338 \[hep-ph\]](#) .
- [46] T. Becher and T. Neumann, (2020), [arXiv:2009.11437 \[hep-ph\]](#) .
- [47] K. Hamilton, P. Nason, E. Re, and G. Zanderighi, *JHEP* **10**, 222 (2013), [arXiv:1309.0017 \[hep-ph\]](#) .
- [48] S. Höche, Y. Li, and S. Prestel, *Phys. Rev.* **D90**, 054011 (2014), [arXiv:1407.3773 \[hep-ph\]](#) .
- [49] P. F. Monni, P. Nason, E. Re, M. Wiesemann, and G. Zanderighi, *JHEP* **05**, 143 (2020), [arXiv:1908.06987 \[hep-ph\]](#) .
- [50] P. F. Monni, E. Re, and M. Wiesemann, *Eur. Phys. J. C* **80**, 1075 (2020), [arXiv:2006.04133 \[hep-ph\]](#) .
- [51] S. Höche, Y. Li, and S. Prestel, *Phys. Rev.* **D91**, 074015 (2015), [arXiv:1405.3607 \[hep-ph\]](#) .
- [52] A. Karlberg, E. Re, and G. Zanderighi, *JHEP* **09**, 134 (2014), [arXiv:1407.2940 \[hep-ph\]](#) .

- [53] S. Alioli, C. W. Bauer, C. Berggren, F. J. Tackmann, and J. R. Walsh, *Phys. Rev.* **D92**, 094020 (2015), [arXiv:1508.01475 \[hep-ph\]](#) .
- [54] W. Astill, W. Bizon, E. Re, and G. Zanderighi, *JHEP* **06**, 154 (2016), [arXiv:1603.01620 \[hep-ph\]](#) .
- [55] W. Astill, W. Bizoń, E. Re, and G. Zanderighi, *JHEP* **11**, 157 (2018), [arXiv:1804.08141 \[hep-ph\]](#) .
- [56] S. Alioli, A. Broggio, S. Kallweit, M. A. Lim, and L. Rottoli, *Phys. Rev.* **D100**, 096016 (2019), [arXiv:1909.02026 \[hep-ph\]](#) .
- [57] S. Alioli, A. Broggio, A. Gavardi, S. Kallweit, M. A. Lim, R. Nagar, D. Napoletano, and L. Rottoli, (2020), [arXiv:2010.10498 \[hep-ph\]](#) .
- [58] D. Lombardi, M. Wiesemann, and G. Zanderighi, (2020), [10.1007/JHEP06\(2021\)095, arXiv:2010.10478 \[hep-ph\]](#) .
- [59] T. Cridge, M. A. Lim, and R. Nagar, (2021), [arXiv:2105.13214 \[hep-ph\]](#) .
- [60] E. Re, M. Wiesemann, and G. Zanderighi, *JHEP* **12**, 121 (2018), [arXiv:1805.09857 \[hep-ph\]](#) .
- [61] L. Buonocore, G. Koole, D. Lombardi, L. Rottoli, M. Wiesemann, and G. Zanderighi, (2021), [arXiv:2108.05337 \[hep-ph\]](#) .
- [62] S. Alioli, A. Broggio, A. Gavardi, S. Kallweit, M. A. Lim, R. Nagar, and D. Napoletano, (2021), [arXiv:2103.01214 \[hep-ph\]](#) .
- [63] J. Mazzitelli, P. F. Monni, P. Nason, E. Re, M. Wiesemann, and G. Zanderighi, (2020), [arXiv:2012.14267 \[hep-ph\]](#) .
- [64] K. Hamilton, P. Nason, C. Oleari, and G. Zanderighi, *JHEP* **05**, 082 (2013), [arXiv:1212.4504 \[hep-ph\]](#) .
- [65] S. Alioli, C. W. Bauer, C. Berggren, F. J. Tackmann, J. R. Walsh, and S. Zuberi, *JHEP* **06**, 089 (2014), [arXiv:1311.0286 \[hep-ph\]](#) .
- [66] J. Campbell and T. Neumann, *JHEP* **12**, 034 (2019), [arXiv:1909.09117 \[hep-ph\]](#) .
- [67] F. Cascioli, P. Maierhöfer, and S. Pozzorini, *Phys. Rev. Lett.* **108**, 111601 (2012), [arXiv:1111.5206 \[hep-ph\]](#) .
- [68] F. Buccioni, S. Pozzorini, and M. Zoller, *Eur. Phys. J.* **C78**, 70 (2018), [arXiv:1710.11452 \[hep-ph\]](#) .
- [69] F. Buccioni, J.-N. Lang, J. M. Lindert, P. Maierhöfer, S. Pozzorini, H. Zhang, and M. F. Zoller, *Eur. Phys. J. C* **79**, 866 (2019), [arXiv:1907.13071 \[hep-ph\]](#) .
- [70] M. Grazzini, S. Kallweit, and M. Wiesemann, *Eur. Phys. J.* **C78**, 537 (2018), [arXiv:1711.06631 \[hep-ph\]](#) .
- [71] <http://matrix.hepforge.org> .
- [72] T. Gehrmann and L. Tancredi, *JHEP* **02**, 004 (2012), [arXiv:1112.1531 \[hep-ph\]](#) .
- [73] P. Nason, *JHEP* **11**, 040 (2004), [arXiv:hep-ph/0409146 \[hep-ph\]](#) .
- [74] P. Nason and G. Ridolfi, *JHEP* **08**, 077 (2006), [arXiv:hep-ph/0606275 \[hep-ph\]](#) .
- [75] S. Frixione, P. Nason, and C. Oleari, *JHEP* **11**, 070 (2007), [arXiv:0709.2092 \[hep-ph\]](#) .
- [76] S. Alioli, P. Nason, C. Oleari, and E. Re, *JHEP* **06**, 043 (2010), [arXiv:1002.2581 \[hep-ph\]](#) .
- [77] U. Baur and E. L. Berger, *Phys. Rev. D* **47**, 4889 (1993).

- [78] D. De Florian and A. Signer, *Eur. Phys. J. C* **16**, 105 (2000), [arXiv:hep-ph/0002138](#) .
- [79] K. Hagiwara, R. D. Peccei, D. Zeppenfeld, and K. Hikasa, *Nucl. Phys. B* **282**, 253 (1987).
- [80] G. Gounaris, J. Layssac, and F. Renard, *Phys. Rev. D* **61**, 073013 (2000), [arXiv:hep-ph/9910395](#) .
- [81] C. Degrande, N. Greiner, W. Kilian, O. Mattelaer, H. Mebane, T. Stelzer, S. Willenbrock, and C. Zhang, *Annals Phys.* **335**, 21 (2013), [arXiv:1205.4231 \[hep-ph\]](#) .
- [82] C. Degrande, *JHEP* **02**, 101 (2014), [arXiv:1308.6323 \[hep-ph\]](#) .
- [83] M. Aaboud *et al.* (ATLAS), *JHEP* **12**, 010 (2018), [arXiv:1810.04995 \[hep-ex\]](#) .
- [84] G. J. Gounaris, J. Layssac, and F. M. Renard, *Phys. Rev. D* **62**, 073013 (2000), [arXiv:hep-ph/0003143](#) .
- [85] T. Gehrmann, E. W. N. Glover, T. Huber, N. Ikizlerli, and C. Studerus, *JHEP* **06**, 094 (2010), [arXiv:1004.3653 \[hep-ph\]](#) .
- [86] P. A. Baikov, K. G. Chetyrkin, A. V. Smirnov, V. A. Smirnov, and M. Steinhauser, *Phys. Rev. Lett.* **102**, 212002 (2009), [arXiv:0902.3519 \[hep-ph\]](#) .
- [87] R. N. Lee, A. V. Smirnov, and V. A. Smirnov, *JHEP* **04**, 020 (2010), [arXiv:1001.2887 \[hep-ph\]](#) .
- [88] R. D. Ball *et al.* (NNPDF), *JHEP* **04**, 040 (2015), [arXiv:1410.8849 \[hep-ph\]](#) .
- [89] G. Aad *et al.* (ATLAS), *Phys. Rev. D* **87**, 112003 (2013), [Erratum: *Phys.Rev.D* 91, 119901 (2015)], [arXiv:1302.1283 \[hep-ex\]](#) .
- [90] S. Frixione, *Phys. Lett. B* **429**, 369 (1998), [arXiv:hep-ph/9801442](#) .
- [91] S. Catani and B. R. Webber, *JHEP* **10**, 005 (1997), [hep-ph/9710333](#) .
- [92] T. Aaltonen *et al.* (CDF), *Phys. Rev. Lett.* **107**, 051802 (2011), [arXiv:1103.2990 \[hep-ex\]](#) .
- [93] V. M. Abazov *et al.* (D0), *Phys. Rev. D* **85**, 052001 (2012), [arXiv:1111.3684 \[hep-ex\]](#) .
- [94] S. Chatrchyan *et al.* (CMS), *Phys. Lett. B* **701**, 535 (2011), [arXiv:1105.2758 \[hep-ex\]](#) .
- [95] G. Aad *et al.* (ATLAS), *Phys. Lett. B* **717**, 49 (2012), [arXiv:1205.2531 \[hep-ex\]](#) .
- [96] S. Chatrchyan *et al.* (CMS), *JHEP* **10**, 164 (2013), [arXiv:1309.1117 \[hep-ex\]](#) .
- [97] S. Chatrchyan *et al.* (CMS), *Phys. Rev. D* **89**, 092005 (2014), [arXiv:1308.6832 \[hep-ex\]](#) .
- [98] V. Khachatryan *et al.* (CMS), *JHEP* **04**, 164 (2015), [arXiv:1502.05664 \[hep-ex\]](#) .
- [99] G. Aad *et al.* (ATLAS), *Phys. Rev. D* **93**, 112002 (2016), [arXiv:1604.05232 \[hep-ex\]](#) .
- [100] V. Khachatryan *et al.* (CMS), *Phys. Lett. B* **760**, 448 (2016), [arXiv:1602.07152 \[hep-ex\]](#) .
- [101] D. R. Green, P. Meade, and M.-A. Pleier, *Rev. Mod. Phys.* **89**, 035008 (2017), [arXiv:1610.07572 \[hep-ex\]](#) .
- [102] T. Sjöstrand, S. Ask, J. R. Christiansen, R. Corke, N. Desai, P. Ilten, S. Mrenna, S. Prestel, C. O. Rasmussen, and P. Z. Skands, *Comput. Phys. Commun.* **191**, 159 (2015), [arXiv:1410.3012 \[hep-ph\]](#) .
- [103] “ATLAS Pythia 8 tunes to 7 TeV datas, ATL-PHYS-PUB-2014-021,” (2014).
- [104] M. Aaboud *et al.* (ATLAS), *Eur. Phys. J. C* **77**, 393 (2017), [arXiv:1704.03848 \[hep-ex\]](#) .
- [105] A. M. Sirunyan *et al.* (CMS), *JHEP* **02**, 074 (2019), [arXiv:1810.00196 \[hep-ex\]](#) .
- [106] M. Aaboud *et al.* (ATLAS), *JHEP* **01**, 126 (2018), [arXiv:1711.03301 \[hep-ex\]](#) .
- [107] A. M. Sirunyan *et al.* (CMS), *Phys. Rev. D* **97**, 092005 (2018), [arXiv:1712.02345 \[hep-ex\]](#) .



- [108] M. Aaboud et al. (ATLAS), *Eur. Phys. J. C* **78**, 18 (2018), [arXiv:1710.11412 \[hep-ex\]](#) .
- [109] A. M. Sirunyan et al. (CMS), *JHEP* **06**, 027 (2018), [arXiv:1801.08427 \[hep-ex\]](#) .
- [110] A. M. Sirunyan et al. (CMS), *JHEP* **03**, 061 (2017), [Erratum: *JHEP* 09, 106 (2017)], [arXiv:1701.02042 \[hep-ex\]](#) .
- [111] M. Aaboud et al. (ATLAS), *JHEP* **10**, 180 (2018), [arXiv:1807.11471 \[hep-ex\]](#) .
- [112] M. Aaboud et al. (ATLAS), *Phys. Rev. D* **96**, 112004 (2017), [arXiv:1706.03948 \[hep-ex\]](#) .
- [113] A. M. Sirunyan et al. (CMS), *JHEP* **10**, 180 (2017), [arXiv:1703.05236 \[hep-ex\]](#) .
- [114] J. Abdallah et al., *Phys. Dark Univ.* **9-10**, 8 (2015), [arXiv:1506.03116 \[hep-ph\]](#) .
- [115] O. Buchmueller, M. J. Dolan, S. A. Malik, and C. McCabe, *JHEP* **01**, 037 (2015), [arXiv:1407.8257 \[hep-ph\]](#) .
- [116] D. Abercrombie et al., *Phys. Dark Univ.* **27**, 100371 (2020), [arXiv:1507.00966 \[hep-ex\]](#) .
- [117] I. Brivio, M. B. Gavela, L. Merlo, K. Mimasu, J. M. No, R. del Rey, and V. Sanz, *Eur. Phys. J. C* **77**, 572 (2017), [arXiv:1701.05379 \[hep-ph\]](#) .
- [118] T. Gleisberg, S. Hoeche, F. Krauss, M. Schonherr, S. Schumann, F. Siegert, and J. Winter, *JHEP* **02**, 007 (2009), [arXiv:0811.4622 \[hep-ph\]](#) .
- [119] E. Bothmann et al. (Sherpa), *SciPost Phys.* **7**, 034 (2019), [arXiv:1905.09127 \[hep-ph\]](#) .